Trends in Electrical Engineering
Volume 1, Issue 1-3 Compilation 2011

STM JOURNALS

Modeling of Fuzzy Logic Controller for Photovoltaic Maximum Power Point Tracker

*Ali M. Eltamaly**
Electrical Engineering Dept., King Saud University, Riyadh, Saudi Arabia

ABSTRACT

In this paper a fuzzy logic controller for maximum power point tracker of photovoltaic (PV) energy system is introduced. This controller uses a boost converter to control the terminal voltage of PV system to work at the maximum power point. The load side consists of battery and control switches to control the power flow from the PV system to the battery and the load. The system is modeled using Matlab/Simulink program. The output power from the PV system with the use of fuzzy controller is compared with the theoretical maximum power from the same system and the power output using the best constant output voltage. The fuzzy controller shows stable operation for different data introduced to the system. It also restrains any overshooting in input or output systems and increases the quantum of energy captured considerably.

Keywords: *Photovoltaic, fuzzy, modeling*

***Author for Correspondence** E-mail: eltamaly@ksu.edu.sa*

INTRODUCTION

The production of electric energy from photovoltaic (PV) sources has a lot of applications, such as in space satellites and orbital stations, solar vehicles, power supply for loads in remote areas, and street lighting systems. PV is environmental friendly and has no emission of harmful gasses as associated with conventional electricity generation.

The power generated from PV is variable with its terminal voltage for each value of radiation and temperature as shown in Figure 1. There is one Maximum Power Point (MPP) associated with each radiation and temperature as shown in Figure 1. Tracking this point to force the PV system to work around it will substantially increase the energy produced. This shows the importance of a MPP Tracker (MPPT). Tracking the MPP needs a fast and smart controller system to counteract the fast changes in weather data or load changes.

MPPT consists of two basic components, dc-dc converter and its controller, which is shown in Figure 2. Many techniqueshave been introduced to catch the MPP. These techniques differ in their complexity, cost, efficiency, response, and robustness. A survey giving a comparison of photovoltaic array MPPT techniques has been discussed earlier in literature [1, 2].

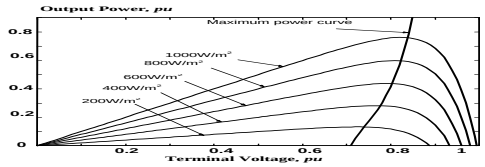

Fig. 1 P-V Characteristics of PV Module.

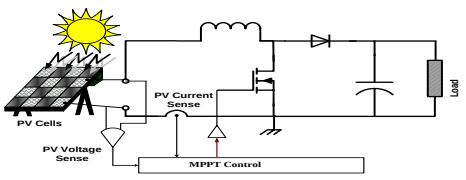

Fig. 2 P-V Energy System with MPPT

In the direct-coupled method [2–4], the PV array is connected directly to the loads without a power modifier. To match the MPPs of the solar array as closely as possible, it is important to choose the solar array characteristics according to the characteristics of the load. The direct-coupled method cannot automatically track the MPPs of the solar array when the insulation, temperature, or, load change.

It is clear from the P-V curve of Figure 1 that the ratio of the array's maximum power voltage, V_{mp}, to its open-circuit voltage, V_{oc}, is approximately constant. So the PV array can be forced to work as a ratio of its open-circuit voltage. The literature reports success of 73–80% from V_{oc} [5–8]. The implementation of this technique can be obtained by temporarily isolating the solar cells from the MPPT, and a V_{oc} measurement is taken. Next, the MPPT calculates the correct operating point and adjusts the array's voltage until the calculated V_{mp} is reached. This technique is very simple to implement but it has two major problems. The first one is the difficulty to choose the optimal value of the constant in the ratio between V_{mp} and V_{oc} and the other one is the momentary interruption of PV power to determine the open-circuit voltage. The latter difficulty can be overcome by using pilot cells.

It is also observed that the relation between the short circuit current and the current associated with the maximum power is approximately constant. So it is possible to use a constant current MPPT algorithm that approximates the MPP current as a constant ratio of the short circuit current [9, 10]. The short-circuit current is measured and the MPP current is calculated, and the PV array output current is then adjusted by the MPPT until the calculated MPP current is reached. This technique faces the same problems as the constant voltage technique. However, constant voltage control is normally favored because the measurement of the open-circuit voltage is much simple than the short circuit current. The momentary interruption in the constant voltage or current can be avoided by using a pilot cell [11].

Another technique called perturb-and-observe (P&O) works by perturbing the system by incrementing the array operating voltage and observing its impact on the array output power. Due to constant step-width the system will face high oscillation especially under unstable environmental conditions. Some techniques use waiting time to avoid high oscillation, however, it also makes the MPPT slower to respond to weather changes. Also, this technique suffers from wrong operation especially in case of multiple local maxima. A lot of modifications for this technique have been presented in literature [12–20].

The incremental conductance (IncCond) method [21–25] is based on comparing the instantaneous panel conductance with the incremental panel conductance. The input impedance of the dc-dc converter is matched with optimum impedance of PV panel. As

noted in literature, this method has a good performance under rapidly changing conditions. But this technique requires more sensing equipment and sophisticated control system.

The parasitic capacitance algorithm [23] is similar to IncCond technique except that the effect of the solar cells' parasitic junction capacitance C_p, which models charge storage in the p-n junctions of the solar cells, is included.

An MPPT approach employing a dither signal superimposed on the updated set point provides the controllability of the amplitude and frequency of the array voltage ripple with respect to the amplitude and frequency of the dither signal. Using the dither signal to properly perturb the MPPT control loop, the power system can operate without a trapped state in which the array voltage is settled far above or below the peak power voltage.

Ripple correlation control (RCC) [26] makes use of ripple to perform MPPT. RCC correlates the time derivative of the time-varying PV array power with the time derivative of the time-varying PV array current or voltage to drive the power gradient to zero, thus reaching the MPP. Simple and inexpensive analog circuits can be used to implement RCC. An example has been performed earlier [27]. Experiments were performed to show that RCC accurately and quickly tracks the MPP, even under varying irradiance levels. The time taken to converge to the MPP is limited by the switching frequency of the power converter and the gain of the RCC circuit. Another advantage of RCC is that it does not require any prior information about the PV array characteristics, making its adaptation to different PV systems straightforward.

The hill climbing technique [26, 28, 29,30] uses a perturbation in the duty ratio of the dc chopper and determines the change in power until the change of power reaches its almost zero value, which is the MPP. The hill climbing technique can be implemented by using a PID controller or by a fuzzy logic controller. This technique requires two sensors to measure the PV array voltage and current from which power is computed or if only one voltage sensor is used, and the PV array current from the PV array voltage is estimated.

Fuzzy logic controller (FLC) has been introduced in many researches [31–36] to force the PV to work around MPP. FLCs have the advantages of working with imprecise inputs, not needing an accurate mathematical model, and handling nonlinearity. A FLC generally consists of three stages: *fuzzification, aggregation,* and *defuzzification*. During fuzzification, numerical input variables are converted into a membership function. The output of the systems has linguistic relations with the inputs of the system. These relations called rules. The output of each rule is a fuzzy set. More than one rule is used to increase

efficiency. Aggregation is the process whereby the output fuzzy sets of each rule are combined to make one output fuzzy set. Afterward, the fuzzy set is defuzzified to a crisp output in the defuzzification process.

MODEL OF THE PROPOSED SYSTEM

In the proposed system, the simulation has been carried out using three different techniques for comparison. In the first technique, a Matlab file has been used to calculate the theoretical MPP of the power curve. In the second technique, a constant terminal voltage of the PV is adjusted. In the last technique, a fuzzy controller has been used to track the MPP. The simulation of the proposed system has been implemented using Matlab/Simulink program as shown in Figure 3. The simulation of the proposed system contains sub-models that can be explained in the following sections:

Photovoltaic Cell Model

The PV cell model is based on the single-diode representation of a silicon photovoltaic cell as illustrated in Figure 4 [37].

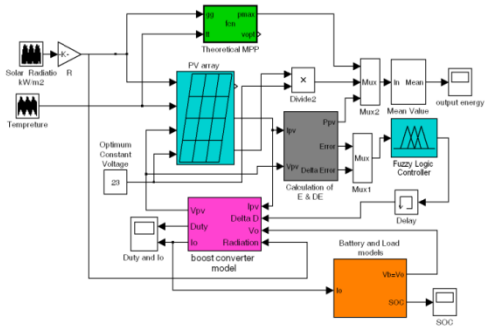

Fig. 3 Simulink Simulation Model of the Proposed System.

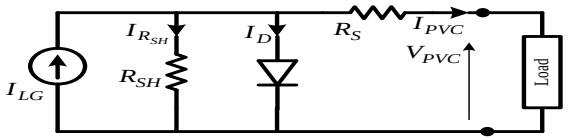

Fig. 4 Equivalent Circuit of Photovoltaic Cell.

The governing equations, which describe the I-V characteristics of a crystalline silicon photovoltaic cell as described in [37], are presented as follows:

The PV cell current, I_{PVC} is obtained by applying Kirchoff's current law to the PV cell shown in Figure 4.

$$I_{\mathrm{PVC}} = I_{\mathrm{LG}} - I_{\mathrm{D}} - I_{\mathrm{R_{SH}}} \quad (1)$$

The light-generated current is given as:

$$I_{\mathrm{LG}} = I_{\mathrm{SCR}} \times G_{\mathrm{N}} + I_t(T_{\mathrm{C}} - T_{\mathrm{r}}) \quad (2)$$

Cell temperature, T_c is obtained from:

$$T_{\mathrm{c}} = T_{\mathrm{a}} + \frac{G}{800}(\mathrm{NOCT} - 25^{\circ}\mathrm{C}) \quad (3)$$

The diode current of the PV cell is:

$$I_{\mathrm{D}} = I_{\mathrm{o}}[e^{\frac{q}{AKT_c}(V_{\mathrm{PVC}} + R_{\mathrm{S}} I_{\mathrm{PVC}})} - 1] \quad (4)$$

The inverse saturation current of the p-n junction is;

$$I_{\mathrm{o}} = I_{\mathrm{or}}\left(\frac{T_{\mathrm{c}}}{T_{\mathrm{r}}}\right)^3 e^{\frac{qE_{\mathrm{G}}}{AK}\left(\frac{1}{T_{\mathrm{r}}}\frac{1}{T_{\mathrm{c}}}\right)} \quad (5)$$

The current due to the shunt resistance is;

$$I_{R_{\mathrm{SH}}} = \frac{V_{\mathrm{PVC}} + I_{\mathrm{PVC}} R_{\mathrm{S}}}{R_{\mathrm{SH}}} \quad (6)$$

Substituting equations 2–6 into equation 1, the cell current can be obtained. From this

equation, it can be seen that the PV cell current is a function of itself, forming an algebraic loop, which can be solved conveniently using Simulink as described in Figure 5.

The module voltage can be obtained by:

$$V_{\mathrm{M}} = V_{\mathrm{PVC}} * N_{\mathrm{SC}} \qquad (7)$$

The module current can be obtained by:

$$I_{\mathrm{M}} = I_{\mathrm{PVC}} * N_{\mathrm{PC}} \qquad (8)$$

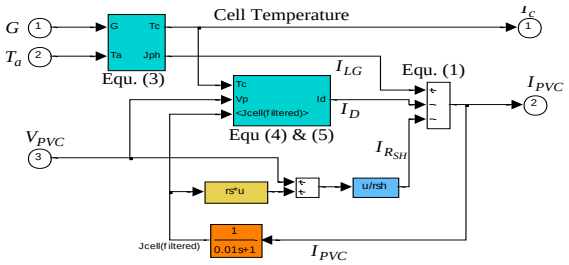

Fig. 5 Simulink Model of PV Cell.

Photovoltaic arrays are represented by the number of modules connected in series, M_S, and the number of modules in parallel, M_P, where the photovoltaic array voltage and current are given as:

$$V_{\mathrm{PV}} = V_{\mathrm{PVC}} * N_{\mathrm{SC}} * M_{\mathrm{S}} \qquad (9)$$

$$I_{\mathrm{PV}} = I_{\mathrm{PVC}} * N_{\mathrm{PC}} * M_{\mathrm{P}} \qquad (10)$$

Battery and Load Model

The battery model has been shown in many literatures and explained in details [38]. The accuracy of this model's data is very important in the whole system. The battery model has two modes of operation; charge and discharge. The battery is in charge mode when the current into the battery is positive, and discharge mode when the current is negative. The battery model has the following input parameters,

(i). Initial state of charge (SOC_l), indicating available charge

(ii). Highest and lowest state of charge, SOC_{H} and SOC_{L} (Wh), respectively

(iii).Number of 2V cells in series

(iv).Charge and discharge battery efficiency; K.

(v). Battery self-discharge rate.

The state of charge has linear relation to the open-circuit terminal voltage of the battery. Initial state of charge can be estimated based on the current open circuit terminal voltage of the battery. The battery with about twice the capacity of average daily load power has been chosen in the simulation.

Control switches are necessary to control the charging and discharging of the battery. These switches are necessary to keep the battery from being overcharged or undercharged, which significantly reduces the battery's life. The control switches are shown in Figure 6. The operating logic used in the control switches is shown in Table I. Switch S_1 will stay ON unless SOC reaches its maximum value, SOC_{H}. Switch S_2 will stay ON unless SOC its minimum value, SOC_{L}.

Table I The Operating Logic Used in the Control Switches.

Mode	S_1	S_2	SOC
1	OFF	ON	SOC = SOC_{H}
2	ON	OFF	SOC = SOC_{L}

3	ON	ON	SOC_L < SOC < SOC_H

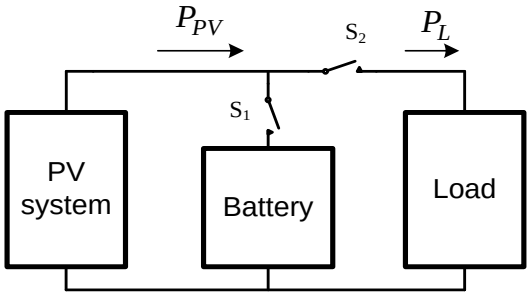

Fig. 6 Block Diagram of Charging Control.

Boost Converter Model

Boost converter block model has been designed as shown in Figure 7. The inputs for this model are the change required in duty ratio, ΔD, Radiation, and I_{PV}. The outputs of this model are the PV output voltage, duty ratio, and the output current. In this model, the duty ratio can take an initial value or it can be set to zero. The value of ΔD is subtracted from the duty ratio to get the new value of the duty ratio depending on the following equation:

$$D(k+1) = D(k) - \Delta D(k) \tag{11}$$

The value of the duty ratio is used to determine the output voltage of the PV array from the following equation:

$$V_{PV} = V_o(1-D) \tag{12}$$

The PV voltage, V_{PV} obtained from (12) and the output current from PV array are used to obtain the PV array output voltage. An efficiency factor can be used to determine the corresponding value of the output power. The output current that feeds the battery and the load can be obtained by dividing the output power on the output voltage, V_O.

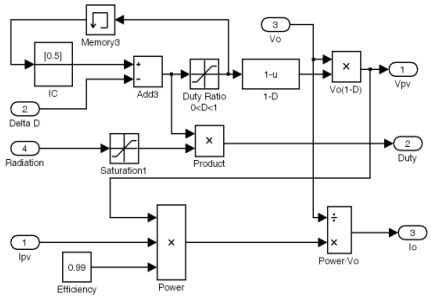

Fig. 7 Simulink Model of the Boost Converter Used in the Simulation.

Model for Calculating *E* and ΔE

The Simulink model of calculating E and ΔE is shown in Figure 8. The input values of this module are I_{PV} and V_{PV}. These values are used to calculate the power from PV array. Then the error signal can be calculated depending on (13). The value of ΔE is calculated as shown in (14).

$$E(n) = \frac{P(n) - p(n-1)}{V(n) - V(n-1)} \tag{13}$$

$$\Delta E(n) = E(n) - E(n-1) \tag{14}$$

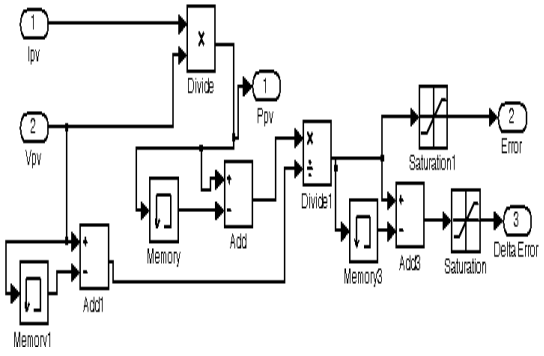

Fig. 8 Simulink Model for Calculating E and ΔE.

Fuzzy Logic Controller Model

The FIS editor is an effective Graphical User Interface (GUI) tool provided with the fuzzy

logic toolbox in Matlab/Simulink to simplify the design of the FLC which can be used in the system under investigation.

The output power from the PV system and the voltage are used to determine the error, E and the change of error, ΔE. In (13) and (14), E and ΔE are based on the range of values of the numerical variable. Predicting the range of error, E, and change of error, $\Delta\Delta E$, depends on the experience of the system designer. These variables are expressed in terms of linguistic variables or labels such as PB (Positive Big), PM (Positive Medium), PS (Positive Small), ZE (Zero), NS (Negative Small), NM (Negative Medium), NB (Negative Big) using the basic fuzzy subset. Each of these acronyms is described by a given mathematical membership function. The membership function is sometimes made less symmetric to give more importance to specific fuzzy levels as in [35] or it can be symmetric as shown in [39] and used here in the current study. The inputs to a MPPT fuzzy logic controller are usually E and ΔE. Once E and ΔE are calculated and converted to the linguistic variables based on membership function as shown in Figure 9, the FLC output, which is typically a change in duty ratio, ΔD of the power converter, can be looked up in a rule base table [1]. FLC membership functions for both inputs and output variables can be used as triangle-shaped function, which is the easiest to implement on the digital control system. The linguistic variables assigned to ΔD for the different combinations of E and ΔE are based on the power converter being used and also on the knowledge of the user.

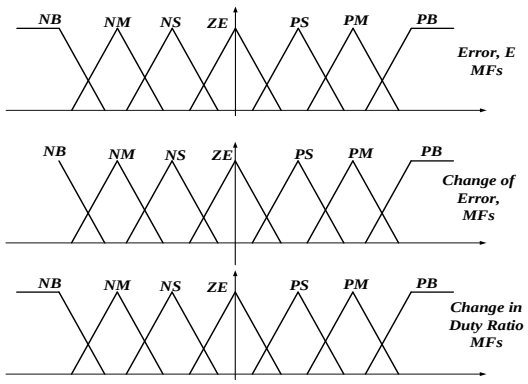

Fig. 9 A Fuzzy System with Two Inputs, one Output, and Seven MFs Each.

These linguistic variables of input and output membership functions are then compared with a set of predesigned values during aggregation stage. The accuracy of the relation between input and output functions determines the appropriate response of the FLC system. The relation between them depends on the experience of the system designer. These relations can be tabulated as shown in Table II [40, 41]. Some researches proportionate these variables to only five fuzzy subset functions as in [33]. Table II can be translated into 49 fuzzy IF-THEN rules to describe the knowledge of control as follows:

R_{25} : *If* E *is NM and* ΔE *is PS then* ΔD *is NS*

R_{63} : *If* E *is PM and* ΔE *is NS then* ΔD *is PS*

….

R_{51} : *If* E *is PS and* ΔE *is NB then* ΔD *is NM*

In the defuzzification stage, the fuzzy logic controller output is converted from a linguistic variable to a numerical variable by using the membership function. This provides an analog

signal which is the change in the duty ratio, ΔD, of the boost converter. This value is subtracted from the previous value of the duty ratio to get its new value as shown in (11).

Defuzzification is for converting the fuzzy subset of control form inference back to values. As the plant usually required a nonfuzzy value of control, a defuzzification stage is needed. Defuzzificaion for this system is the height method. The height method is both very simple and very fast. The height defuzzification method in a system of rules is formally given by (15):

$$\Delta D = \left(\sum_{k=1}^{m} c(k) * W_k \right) / \sum_{k=1}^{n} W_K \qquad (15)$$

where ΔD = change of control output
$c(k)$ = peak value of each output
W_k = height of rule k.

The relation between the inputs and the output of the fuzzy controller can be represented as a 3D drawing, called surface function, as shown in Figure 10. It is clear that the surface function is approximately smooth, which enhances the stability of the fuzzy system.

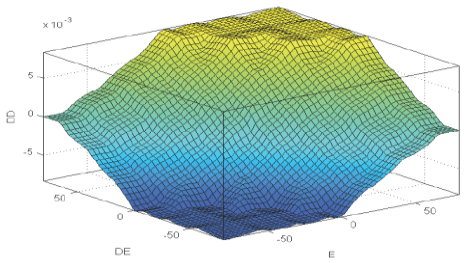

Fig. 10 Surface Function of the Proposed FLC.

SIMULATION RESULTS

The radiation and temperature data used in the simulation are from realistic hourly data of the Riyadh city of Saudi Arabia. These data are concentrated in a narrow range of time (4 sec), which improves the robustness of the fuzzy controlled system. Six PV-modules have been used in the simulation with specifications shown in the Appendix. The simulation is carried out with FLC and constant voltage technique for the purpose of comparisons. These two MPPT techniques have been compared with theoretical maximum power from a PV module using a Matlab file. The load is connected to a PV array through a battery. Figure 11 shows the solar radiation used in the simulation in the first trace. In the second trace, the output power from the for FLC and constant voltage MPPT technique is compared with the theoretical value of MPPT. It is clear from second trace that, the power output with FLC is following the theoretical MPP exactly but the output power with constant voltage control is considerably lower than that associated with FLC. Moreover, FLC can restrain any overshooting in the input or output variables.

Third trace of Figure 11 shows the value of change of control output, ΔD which is the output from FLC. This value can be used to modulate the value of the duty ratio. Fourth trace of Figure 11 shows the duty ratio of the boost converter. Fifth and sixth traces of Figure 11 show the error function, E and the change in error, ΔE.

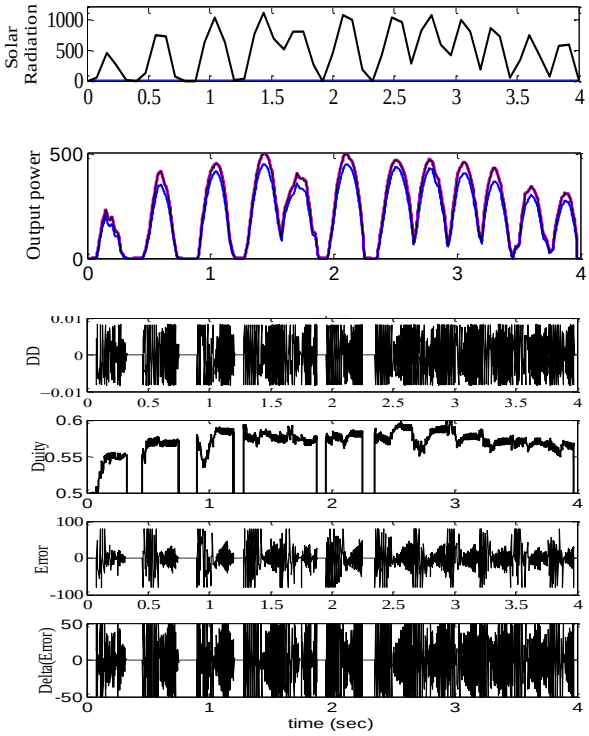

Fig. 11 Simulation Results of the Proposed FLC System.

Output power from the PV system using FLC and constant voltage along with the theoretical MPPT are shown in Figure 12 for the purpose of comparison. It is clear from Figure 12 that the output power associated with FLC system follows the theoretical MPPPT exactly, which proves the superiority of the system.

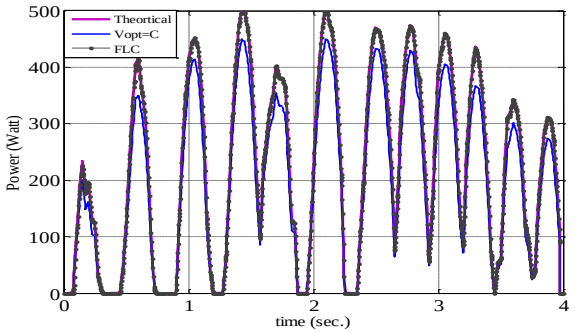

Fig. 12 The Output Power from PV System using FLC and Constant Voltage Along with the Theoretical MPPT.

Magnified images for the E, ΔE, ΔD, D, and optimum voltage, V_{PV}, are shown in Figure 13 to simplify the tracking of the logic of the FLC system. The logic shown in Table II can be explained with the help of this figure.

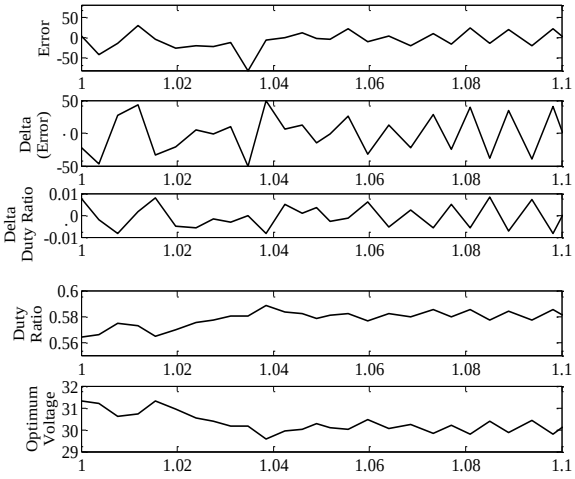

Fig. 13 Simulation Results of the FLC System.

Table II Rules for a Fuzzy System with Two Inputs and One Output with 7-Membership Functions.

Δ E E	NB	N M	NS	ZE	PS	PM	PB
NB	NB	NB	NB	NB	N M	NS	ZE
NM	NB	NB	NB	N	NS	ZE	PS

				M			
NS	NB	NB	N M	NS	ZE	PS	PM
ZE	NB	N M	NS	ZE	PS	PM	PB
PS	N M	NS	ZE	PS	PM	PB	PB
PM	NS	ZE	PS	PM	PB	PB	PB
PB	ZE	PS	PM	PB	PB	PB	PB

CONCLUSIONS

The generated power from the photovoltaic cell changes with the operating voltage of the PV cell. There is a MPP at a certain voltage of the PV cells. MPPT is used to track this point. Tracking the MPP by using the fuzzy logic control provides an accurate tracking mechanism for the maximum power point even in highly changing weather conditions. Fuzzy logic control system restrains any overshooting in input or output systems and increases the amount of the energy captured considerably.

FUTURE WORK

This fuzzy control system will be implemented in FPGA board. Also, the system will be connected to a three-phase induction motor to feed certain loads and the control of the induction motor will be carried out by using fuzzy logic. This work was financially supported by NPST program by King Saud UniversityProject: Number 08-ENE226-02.\\

ACKNOWLEDGMENTS

This work was financially supported by NPST program by King Saud University Project: Number 08 ENE226-02.

REFERENCES

1. Esram T. and Chapman P. L. *IEEE Transactions on Energy Conversion* June 2007. 22. 2. 439–449p.
2. Salas V. Olías E., Barrado A. et al. *Solar Energy Materials and Solar Cells* 6 July 2006. 90. Issue 11. 1555–1578p.
2. Balouktsis A., Karapantsios T. D., Anastasiou K. et al. *International Journal of Photoenergy* 2006. 27274. 1–7p.
3. Khouzam K. Y. *IEEE Transactions on Energy Conversion* June 1990. 5. 2. 265–271p.
4. Anis W. R. and Metwally H. M. B. *Solar Energy* 1994. 53. 4. 369–377p.
5. Dehbonei Masoum H. and Fuchs E. F. *IEEE Transactions on Energy Conversion* Dec. 2002. 17. 4. 514–522p.
6. Noh H. J., Lee D. Y. and Hyun D. S. in *Proceedings of* 28th *Annual Conference* of the IEEE *Industrial* Electronics *Society* 2002. 1113–1118p.
7. Kobayashi K., Matsuo H. and Sekine Y. in *Proceedings* of 35th *Annual IEEE Power Electronics Specialists Conference* 2004. 2147–2151p.
8. Bekker B. and Beukes H. J. *7th AFRICON Conference in Africa* 2004. 1125–1129p.

9. Mutoh N., Matuo T., Okada K. et al. in Proceedings of 33rd *Annual IEEE Power Electronics Specialists Conference* 2002. 1489–1494p.
10. Yuvarajan S. and Xu S. in Proceedings of *International Symposium* on *Circuits* and *Systems* 2003. III-399–III-402p.
11. Veerachary M., Senjyu T., Uezato K. *IEEE Transactions On Aerospace and Electronic Systems* Jan. 2002. 38. 1. 262–270p.
12. Fermia N., Granozio D., Petrone G. et al. *IEEE Transactions on Aerospace and Electronic Systems* July 2007. 43. 3. 934–950p.
13. Chiang M. L., Hua C. C. and Lin J. R. in Proceeding of *Energy Conversion Conference* and *Exposition* 2002. 311–315p.
14. Wu. W., Pongratananukul N., Qiu W. et al. *Applied Power Electronics Conference and Exposition* 2003.
15. Hsiao Y. T. and Chen C. H. *in Record 37th IAS Annual Meeting Industrial Application Conference* 2002. 1035–1040p.
16. Jung Y., Yu G., Choi J. et al. in Conf. Record *29th IEEE Photovoltaic Specialists Conference*. 2002. 1410–1413p.
17. Jain S. and Agarwal V. *IEEE Power Electronics Letters* Mar. 2004. 2. 1. 16–19p.
18. Tafticht T. and Agbossou K. inIEEE Canadian *Conference* on *Electrical* and *Computer Engineering* 2004. 1123–1126p.
19. Femia N., Petrone G., Spagnuolo G.et al. *IEEE Transactions on Power Electronics* Jul. 2005. 20. 4. 963–973p.
20. Wolfs P. J. and Tang L. in Proceedings of *36th Power Electronics Specialists Conference* 2005. 165–171p.
21. Kobayashi K., Takano I. and Sawada Y. in *IEEE Power & Energy Society General Meeting* 2003. 2612–2617p.
22. Wu W., Pongratananukul N., Qiu W. et al. *Eighteenth Annual IEEE Applied Power Electronics Conference and Exposition* 2003. 525–530p.
23. Lee Jae Ho, Bae HyunSu and Cho Bo Hyung. *Power Electronics and Motion Control Conference* 2006. EPE-PEMC 2006. 12th International at Portoroz. 603–607p.
24. Kouta J., El-Ali A., Moubayed N. et al. Available at http://www.icrepq.com/icrepq-08/281-kouta.pdf.
25. Eltamaly Ali M., El-Tamaly H. H. and Enjeti P. *2nd Minia International Conference for Advanced Trends in Engineering* March 2002. (MICATE'2002) Elminia. Egypt. 1618p.
26. Kimball J. W. Krein P. T. *IEEE Power Electronics Specialists Conference* 2007. Orlando. FL. 1690–1694p.
27. Lalounia S., Rekiouaa D., Rekiouaa T. et al. *Journal of Power Sources* 2009. 193. 899–907p.

28. Veerachary M., Senjyu T. and Uezato K. in *IEE Proceedings Electric Power Applications* 2001. 494–502p.
29. Xiao W. and Dunford W. G. *in Proc. IEEE 35th Annual Power Electronics Specialists Conference* 2004. 1957–1963p.
30. Liu Fangrui, Kang Yong, Zhang Yu. *3rd IEEE Conference on Industrial Electronics and Applications* 2008. Singapore. ICIEA 804–807p.
31. Gounden N. Ammasai, Peter Sabitha Ann, Nallandula Himaja. *Renewable Energy Journal* 2009. 34. 909–915p.
32. Ben Salah Chokri, Chaabenea Maher and Ben Ammara Mohsen. *Renewable Energy* 2008. 33. 993–1001p.
33. Altasa I. H. and Sharaf A. M. *Renewable Energy* 2008. 33. 388–399p.
34. Khaehintung N., Pramotung K., Tuvirat B.et al. *in Proc. 30th Annual Conference of IEEE Industrial Electronics Society* 2004. 2673–2678p.
35. Karlis A. D., Kottas T. L. and Boutalisb Y. S. *Electric Power Systems Research* March 2007. 3–4. 315–327p.
36. Veerachary M., Senjyu T. and Uezato K. *IEEE Transactions on Industrial Electronics* Aug. 2003. 50. 4. 749–758p.
37. Markvart Tom and Castafier Luis. *Solar Cells: Materials, Manufacture and Operation*, Elsevier Publishing Co. ISBN-13:978-1-85617-457-1. 2005.
38. Castan˜er Luis and Silvestre Santiago. *Modelling Photovoltaic Systems using PSpice*. John Wiley & Sons Ltd. The Atrium. Southern Gate. Chichester. West Sussex. UK. ISBN 0-470-845279. 2002.
39. Larbes C. Aı¨t Cheikh* S. M., Obeidi T. et al. *Renewable Energy* 2009. 34. 2093–2100p.
40. Datta Manoj, Senjyu Tomonobu, Yona Atsushi et al. *2nd IEEE International Conference on Power and Energy* December 1–3 2008. Johor Baharu. Malaysia.
41. Wang Yiwang and Cao Fengwen. *Power and Energy Engineering* Conference 2009. Asia-Pacific. Wuhan. 1–4p.

LIST OF SYMBOLS

I_{PVC} : PV cell current

I_{LG} : The light-generated current

I_D : Diode current (A)

$I_{R_{SH}}$: shunt circuit resistance current.

G : Irradiance (W/m^2)
T_a : Ambient Temperature (°K)
T_c : Cell Temperature (°K)
V_{PV} : Array Voltage (V)
I_{PV} : Array Current (A)
I_{SCR} : short ircuit Current under STC=4.92A

I_t : Short-circuit current temperature coeff.= $1.7e^{-3}$ A/°K

T_R : Cell reference Temperature (°K)

NOCT :Normal operation cell temperature =43 °K
A : Diode ideality factor = 1.043

K : Poltizman constant
q : Electron Charge
I_o : The inverse saturation current

R_S : Series resistance (Ω)

R_{SH} : Shunt resistance (Ω)

I_{or} : diode saturation current at reference temp. = $3.047e^{-7}$

E_G : Band gap for semiconductor material silicon = 1.11 eV

N_{SC} : Number of cells in series in one module

N_{PC} : Number of cells in parallel.

M_S : Number of modules in series.

M_P : Number of modules in parallel.

